Rail corrugation: "one hundred years of solitude"?

L.Afferrante[1], M.Ciavarella[1,2]

[1]CEMEC-PoliBA - Via Re David 200, Politecnico di Bari, 70124 Bari, Italy

[2]LMS - Ecole Polytechnique, Palaiseaux-Paris, France

April 9, 2008

Abstract

Rail corrugation has been noticed at least for 100 years, but (particularly short pitch one in the range $20 \div 80$ mm) has been considered an enigma because measured corrugation wavelength did not relate well with wear-instability models. We suggest this is mainly due to the intrinsic large number of parameters which has resulted in many independent efforts to generate models, many false beleives, the difficulty to collect experimental evidence, and the lack of sufficient comparisons between models which has quite clearly not permitted to elucidate the main ingredients of the problem. In particular, while very complex models have been generated, often they are quite naive in one or more assumptions.

Recently, we have shown a satisfactory explanation of short pitch corrugation can be achieved with quite simple models, which we improve here to consider transient contact dynamic effects in partial slip and 3D configurations. It is found that for nearly circular contact, a closed form simple solution that corrugation is possible in the range $300 \div 600$ Hz, in agreement with experiments, depending on normal load, creepage ratio, shape of the contact area.

There is no need therefore to call for effects of discrete supports and the associated pinned-pinned resonance, in generating corrugation, as this is not supported by many experimental data. We prefer to keep a prudent and agnostic view on it, because most models in support of its importance do not correctly model its effect, which is extremely difficult to deal with.

Keywords: short pitch corrugation, rolling contact, wear, friction instabilities.

1 Introduction

Corrugations caused by the action of the railways wheels is a phenomenon observed throughout railways history (i.e. at least in the last 100 years) but not fully understood (Grassie and Kalousek, 1993) particularly for short-pitch rail corrugation ("roaring rails") in the range of $20 \div 80$ mm wavelength. Most available data seem to show a non-linearly increasing wavelength with speed, ie an almost fixed-wavelength and not fixed-frequency feature (see figure 1 adapted from figure 1 of Bhaskar *et al.* (1997), with quite a lot of data in BR reports in 1911, David Harrison's Cambridge Ph.D. thesis (1979) and the Vancouver SkyTrain data). Instead, most models generally obtain a resonance on the system, the most obvious being the vertical direction one, like in the early Hertz spring "contact resonance" mechanism of Carson and Johnson (1971) and Johnson and Gray (1975). In the range of frequency of short-pitch corrugation, the normal force has its peak near the crest of the corrugation, and hence a mechanism of

plastic impacts cannot be active, as confirmed by evidence suggesting plastic deformation (and sometimes martensitic transformations) occurs on the peaks but not on the troughs (Frederick, 1986), and instead evidence of slip and wear. However, he also reported open hearth rail steel is much less prone to corrugate than Acid Bessemer, and in general high plastic deformation resistant material show corrugation quickly, although the increase of wear resistance slows the rate of formation. Therefore, a more complete model probably should consider competing plastic and wear mechanisms.

The first simple model involving a differential wear mechanism with longitudinal creepage like in braking or acceleration, was suggested by Grassie and Johnson (1985), but failed to explain corrugation, since reported to act as *suppressing* corrugation, and by now after about 15 years or research in Cambridge and at BR, the puzzle of rail corrugation started to be spoken of as an "enigma". However, Ciavarella and Barber (2008) recently suggested that this conclusion comes from erroneously assuming constant longitudinal creepage and when the inertia of the wheel and the rotational dynamics of the system are considered, a much better qualitative agreement with experimental evidence is immediately found.

Later, BR introduced quite a few innovations in the Frederick model (1986), with discrete supports, a sort of perturbation approach using complex transfer functions, and a detailed treatment of the receptances in both lateral longitudinal and vertical direction, including also the mass of the wheel (as a concentrated mass) in the analysis, hence a model not only satisfying the requirements but much richer than Ciavarella and Barber (2008). Frederick did find a few possible regimes of corrugation, but still he made a few assumptions and a quite crude treatment for the discrete support effect, and hence jumped to the conclusion that the dominant mechanism would be lateral corrugation at the pinned-pinned resonance at about $800 - 1100\ Hz$ in most railways systems, in which the rail vibrates almost as if it were a beam pinned at sleepers, which is strictly due to the effect of including the discrete nature of supports. Later, many models assume this is a needed ingredient for corrugation, and lately has actually been associated to a firm and definitive source of short-pitch corrugation in a recent review by Grassie (2005):- *"...it is now clear that the wavelength-fixing mechanism for this type of corrugation, on which the author believed it prudent to hold an "agnostic" view in 1993 [7], is indeed the so-called "pinned-pinned" resonance, in which the rail vibrates as if pinned at the sleepers. This is demonstrated convincingly by the linear modelling of Hempelmann from TUB....The frequency of this mode is typically about 800 Hz in the UK, for a sleeper spacing of 0.75 m and 56 kg/m rail, whereas in much of continental Europe it is more commonly about 1200 Hz because of the closer sleeper spacing (0.6 m) and heavier rail section (60 kg/m) [10]. The search for a mechanism that would give a constant wavelength, which had been central to the joint British Rail Research and Cambridge University research project in the 1970s and 1980s, is evidently a chimera that had emerged because types of corrugation that arise from different mechanisms were then believed to have had the same cause.*

However, we think that it is still prudent to keep an "agnostic view" since the original data collected by British Rail Research and Cambridge University, which are probably still the most reliable around, are still not explained at all in terms of pinned-pinned resonance, as it is clear from figure 1. Also, short-pitch corrugation appeared very strongly on Vancouver SkyTrain which has not a typical discrete support, and indeed did not change when the spacing of support changed. Indeed, we believe that the conclusions about pinned-pinned modes are affected by three facts:-

1) models with discrete supports (Frederick 1986, Hempelmann and Knothe, 1996, Hempelmann, 1994), in the attempt to introduce their effect, generally use local eigenvalue analysis, which means that they assume a steady state is reached like if the local receptance were valid for an infinite length. This exaggerates the amplification of

normal load (or of lateral loads, or both) above sleepers by an unknown factor (for example, from Grassie *et al.*, 1982 we estimated the error can be easily a factor 2 if not larger[1]). This clearly has the effect to exaggerate the possibility of corrugation due to pinned-pinned resonance, particularly in lateral direction since in longitudinal direction the phase appears not appropriate for corrugation (Frederick 1986).

2) models with continuum support (Grassie and Johnson, 1985, Bhaskar *et al.*, 1997, Meehan *et al.*, 2005, Wu and Thompson, 2005, for example) have partly failed in quantitative prediction of wavelength only because of the erroneous tangential dynamics assumptions; when the wheel inertia and the transient contact mechanics effects are considered, like shown in a recent model (Ciavarella and Barber, 2008) using a continuum description of the rail (hence neglecting pinned-pinned resonance), the results seem to show a few possible regimes where many wavelengths are unstable at low speed, and an apparent regime of highest growth just above 400 Hz, not too remote from the experimental evidence

3) proper parametric resonance models (Wu and Thompson (2006), Sheng *et al.* (2006), Wu and Thompson (2004)). Only recently, proper parametric resonance models on the system with discrete supports have been attempted, but mostly they deal with noise rather than corrugation. The effects are very difficult even to describe and to study, they depend on stiffness of the pad, a peak with the "local" calculation becomes distinctly mid-sleepers at frequencies actually higher than the pinned-pinned resonance ($1200 - 1400$ Hz) rather than that at above sleepers. The authors talk of parametric effects being important at high speeds, but really the "local" approach should be correct when the ratio wavelength of corrugation over sleepers distance is small. Hence, the very short wavelengths should be correctly modelled with the local approach. However, the transient dynamic effects become extremely difficult to deal with.

—

So with this sort of background, we decided to look at the simplest possible model, given we are not in a position to easily check results with apparently more sophisticated numerical simulations. To us, a lot more validation is needed for even the simplest of these numerical models, and our own efforts to produce clean and closed form solutions is also along the lines of extending the possibilities to check these models. Incidentally, our models are so simple as to permit an almost closed form manipulation of the resulting behaviour, so it is extremely simple to make parametric studies.

With respect to the previous contributions, here we improve the treatment from Ciavarella and Barber (2008) as they assumed a simple full stick Winkler contact mechanics. Far from having the ambition to give a definitive and final word on this complicated problem, we shall simply elucidate the effect of contact geometry in the likely short-pitch corrugation regime, removing the Winkler approximation, and using a continuous analytical solution approximately valid for 3D elliptical contact areas, and in partial slip. To simplify the discussion, we shall use an extremely simplified vertical receptance model, but valid in the frequency range greater than 500 Hz, of course under the assumption of neglecting pinned-pinned resonance due to discrete supports. In doing the approximate 3D treatment, we differ from a previous attempt by Bhaskar *et al.* (1997) who used a model validated only for variations of tangential load.

[1]In Grassie *et al.* (1982), calculated dynamic loads for a continuous model of Fig.3 without discrete supports are compared with measurements by load measuring wheel in Fig.12. The highest load is at about 1000Hz, about 2.8 times higher than at 600Hz. We estimated the same increase to be a factor 5 with a "local" use of receptances as in the Frederick or Hempelmann "moving perturbation" models, for a BR track with the standard "Grassie" 280MN/m stiff pad.

2 The model

The model under investigation is initially that proposed in Barber *et al.* (2008). For a wheel rotating over a corrugated rail translating with velocity V, and concentrating all the elastic deformation in the wheel (we shall use an equivalent modulus for the wheel and treat the rail as rigid, in the tangential direction), we can define a slip velocity in terms of the tangential displacements of the contacting points u_x. The condition of zero slip (assuming the coefficient of friction is sufficiently high to prevent slip occurring anywhere), gives a partial differential equation for u_x. Barber *et al.* (2008) have shown how to find a small perturbation solution of this, i.e. assuming that $\Omega(t)$ is a known function of the form

$$\Omega(t) = \Omega_0 + \Omega_1 \exp(\imath\omega t) \; . \tag{1}$$

and every other quantity has a steady state and an oscillating component. For example, the normal and tangential forces P, Q have the sinusoidal form

$$P(t) = P_0 + P_1 \exp(\imath\omega t) \; ; \quad Q(t) = Q_0 + Q_1 \exp(\imath\omega t) \; , \tag{2}$$

where P_0, P_1, Q_0, Q_1 are constants and $P_1 \ll P_0, Q_1 \ll Q_0$. Also, the instantaneous contact semi-width a is

$$a(t) = a_0 + a_1 \exp(\imath\omega t) \; , \tag{3}$$

where

$$a_0 = \sqrt{\frac{4P_0R}{\pi E^*}} \; ; \quad a_1 = P_1 \frac{\partial a}{\partial P} = P_1 \sqrt{\frac{R}{P_0 \pi E^*}} = \frac{P_1 a_0}{2P_0} \; . \tag{4}$$

and E^* is the composite modulus

$$\frac{1}{E^*} = \frac{(1-\nu_1^2)}{E_1} + \frac{(1-\nu_2^2)}{E_2} \tag{5}$$

At any given time t, contact extends over $-a(t) < x < a(t)$ and the contact pressure is bounded at the leading edge $x = -a(t)$ and singular at the trailing edge $x = a(t)$. Barber *et al.* (2008) show how to produce a solution that is bounded at the leading edge $x = -a$ and singular at the trailing edge $x = a$, by superposing a series of solutions of a special form. The derivation is somewhat lengthy, and the reader is referred to the paper for details. The results can be rewritten concisely in terms of tangential load and energy dissipation perturbation in full stick, as

$$Q_1 = Q_P P_1 + Q_\Omega \Omega_1 \; ; \; W_1 = W_P P_1 + W_\Omega \Omega_1 \; , \tag{6}$$

where

$$\frac{Q_P(\zeta)}{Q_P^0} = 1 + \frac{\imath\zeta}{2\pi D(\zeta)} I_1\left(\frac{\zeta}{2}\right)\left[1 + \ln\left(\frac{a_0}{2d}\right)\right] ; \qquad \frac{Q_\Omega(\zeta)}{Q_\Omega^0} = \frac{I_1\left(\frac{\zeta}{2}\right)}{\pi D(\zeta)} \tag{7}$$

$$\frac{W_P(\zeta)}{V\epsilon_0 Q_P^0} = 1 + \frac{\imath\zeta}{D(\zeta)} J_0\left(\frac{\zeta}{2}\right)\left[1 + \ln\left(\frac{a_0}{2d}\right)\right] ; \qquad \frac{W_\Omega(\zeta)}{2V\epsilon_0 Q_\Omega^0} = \frac{J_0\left(\frac{\zeta}{2}\right)}{D(\zeta)} \tag{8}$$

where ϵ_0 is the mean creep ratio and the function $D(\zeta)$, which has a crucial role in transient effects, is also dependent on the factor $\ln\left(\frac{a_0}{2d}\right)$, where d can be interpreted as a measure of the finite dimensions of the contacting body (e.g. the radius of a cylinder),

$$D(\zeta) = J_0\left(\frac{\zeta}{2}\right) - \frac{\imath\zeta}{2\pi} I_1\left(\frac{\zeta}{2}\right) \ln\left(\frac{a_0}{2d}\right) \tag{9}$$

and $Q_P^0 = \frac{\epsilon_0}{a_0/R}$, $Q_\Omega^0 = -\frac{\pi E^* R a_0}{2V}$ are respectively the values of the functions $Q_P(\zeta), Q_\Omega(\zeta)$ in limit of $\zeta \to 0$, where

$$\zeta = \frac{2\omega a_0}{V} \tag{10}$$

and $I_1(p)$ is an integral which can be written in terms of Bessel functions

$$I_1(p) = \int_{-1}^{1} \exp(\imath p s) \sqrt{\frac{1+s}{1-s}} ds = \pi \left\{ J_0(p) + \imath J_1(p) \right\} \ . \tag{11}$$

In this same limit $\zeta \to 0$, the results of this model coincide with previous results obtained by Ciavarella and Afferrante (2008) already perturbing Carter's (1926) steady state solution.

2.1 Partial slip 3D solution

The zero-th order coefficient of Carter's solution can be equally simply obtained in the partial slip conditions, not just in full stick. Full stick conditions were assumed only because the full continuum solution under partial slip would involve computation of the energy dissipation in the slip area, by evaluating directly the product of local shear traction, and local microslip. We can however neglect further changes in the ζ dependence of the solution, and hence obtain the coefficients in partial slip. In doing this, we shall also profit to add also the 3D effect, since a full perturbed solution of 3D continuum solution is not viable. In the next paragraph, hence, we shall replace the zero-th order coefficients in the present solution, with the zero-th order coefficients of the Carter equivalent solution in 3D, with partial slip.

Bhaskar *et al.* (1997) estimate the effect of a true elliptical Hertzian contact by introducing the equivalent of the Carter's solution in 3D. which is the case of pure longitudinal creep ratio (we assume no lateral creep) (Bhaskar *et al.* 1997, eqt.5a), in terms of the tractive ratio $\tau = Q/\mu P$

$$\epsilon = \epsilon_{\max} \left[1 - (1-\tau)^{1/3} \right] \tag{12}$$

where Q is the resulting tangential force which is only in the x-direction, and $\epsilon_{\max}$ is given by[2]

$$\epsilon_{\max} = \frac{3\mu}{C_{00}} \left[\frac{16P}{9(1-\nu)^2 R_e^2 G} \right]^{1/3} \tag{13}$$

with the Kalker's creep coefficient expressed approximately as a function of a/b

$$C_{00} = 2.84 + 1.2\frac{a}{b} \approx 2.84 + 1.2 \left(\frac{R}{R_r} \right)^{2/3} \tag{14}$$

where R is the rolling radius of the wheel, R_r the relative radius of curvature between the wheel and the rail and $R_e = \sqrt{R_r R}$. Now, (12) can be rewritten as

$$Q = \mu P \left(1 - \frac{(\epsilon_{\max} - \epsilon)^3}{\epsilon_{\max}^3} \right)$$

[2]We are defining the Kalker coefficients as positive, for simplicity, and hence change the sign of the creep-load relationships as more commonly found in the literature.

It then follows that the dissipation is

$$W = V\epsilon Q = \mu PV\left(1-\frac{\Omega R}{V}\right)\left(1-\frac{\left(\epsilon_{\max}-\left(1-\frac{\Omega R}{V}\right)\right)^3}{\epsilon_{\max}^3}\right), \tag{15}$$

where remember that $\epsilon_{\max}$ is a function of P (according to (13)). Hence, by differentiation, we obtain the zero-th order factors, which now depend on tractive ratio τ (or equivalently, the ratio $\frac{\epsilon_0}{\epsilon_{\max}}$), but also on ϵ_0 separately, as as well as friction coefficient

$$Q^0_{P,3D} = \left.\frac{\partial Q}{\partial P}\right|_{P_0,\Omega_0} = \frac{2\mu\epsilon_0}{\epsilon_{\max}}\left(1-\frac{\epsilon_0}{2\epsilon_{\max}}\right); \tag{16}$$

$$Q^0_{\Omega,3D} = \left.\frac{\partial Q}{\partial \Omega}\right|_{P_0,\Omega_0} = -\frac{3\mu RP_0}{V\epsilon_{\max}}\left(1-\frac{\epsilon_0}{\epsilon_{\max}}\right)^2; \tag{17}$$

$$W^0_{P,3D} = \left.\frac{\partial W}{\partial P}\right|_{P_0,\Omega_0} = \frac{2\mu V\epsilon_0^2}{\epsilon_{\max}}\left(1-\frac{\epsilon_0}{2\epsilon_{\max}}\right) = V\epsilon_0 Q^0_{P,3D}; \tag{18}$$

$$W^0_{\Omega,3D} = \left.\frac{\partial W}{\partial \Omega}\right|_{P_0,\Omega_0} = 2\epsilon_0 V Q^0_{\Omega,3D}\left[1+\beta\left(\frac{\epsilon_0}{\epsilon_{\max}}\right)\right]. \tag{19}$$

where

$$\beta\left(\frac{\epsilon_0}{\epsilon_{\max}}\right) = \frac{\frac{\epsilon_0}{2\epsilon_{\max}}\left(1-\frac{2\epsilon_0}{3\epsilon_{\max}}\right)}{\left(1-\frac{\epsilon_0}{\epsilon_{\max}}\right)^2} \tag{20}$$

In Ciavarella and Barber (2008) a Winkler model was used, with Winkler modulus k_q chosen to fit some equations of the Carter solution. However, it resulted that the freedom to choose the Winkler modulus is sufficient to match the steady state solution, but this choice does *not* fit the full perturbed solution not even in the limit $\zeta \to 0$. Specifically, if we fitted the equation for Q_Ω, the other two perturbation coefficients Q_P , W_P could not be matched by a factor 2.

This means the transient effects are more complicated than what a pure Winkler model can predict, and indeed similar difficulties have been noticed also by Alonso and Gimenez (2007) tuning the Winkler-based code FASTSIM to the exact results of CONTACT. The full perturbation of the continuum CONTACT code has been done by Gross-Thebing (1994), and indeed the generalized Kalker coefficients that he defines depend on many factors (geometry of the contact, Poisson's ratio, etc.), and even to get the tangential load (either longitudinal or lateral), the perturbation with respect to many parameters is needed in 3D (longitudinal or lateral creepage, contact area ellipse semi-diameters, peak pressure, etc). Unfortunately Gross-Thebing gives very limited results for the energy dissipation which he finds correctly as the integral of density over the slip area.

A possibility that is explored here is changing the ratio $\alpha = \frac{a_0}{2d}$ and then assume that all the other relationships remain unchanged from the 2D solution, so that (7,8) can be rewritten as

$$\hat{Q}_P(\zeta,\alpha) = \frac{Q_P(\zeta,\alpha)}{Q^0_{P,3D}} = 1+\frac{\imath\zeta\left[1+\ln(\alpha)\right]}{2\pi D(\zeta,\alpha)} I_1\left(\frac{\zeta}{2}\right); \qquad \hat{Q}_\Omega(\zeta,\alpha) = \frac{Q_\Omega(\zeta,\alpha)}{Q^0_{\Omega,3D}} = \frac{I_1\left(\frac{\zeta}{2}\right)}{\pi D(\zeta,\alpha)} \tag{21}$$

$$\hat{W}_P(\zeta,\alpha) = \frac{W_P(\zeta,\alpha)}{W^0_{P,3D}} = 1+\frac{\imath\zeta\left[1+\ln(\alpha)\right]}{D(\zeta,\alpha)} J_0\left(\frac{\zeta}{2}\right); \qquad \hat{W}_\Omega(\zeta,\alpha) = \frac{W_\Omega(\zeta,\alpha)}{W^0_{\Omega,3D}} = \frac{J_0\left(\frac{\zeta}{2}\right)}{D(\zeta,\alpha)} \tag{22}$$

where now the zero-th order factors $Q^0_{P,3D}, Q^0_{\Omega,3D}, W^0_{P,3D}, W^0_{\Omega,3D}$ are obtained from the full partial slip 3D Carter solution (eq. (16-19)), so depend on the ellipticity of the contact, the tractive ratio τ (or equivalently, the ratio $\frac{\epsilon_0}{\epsilon_{\max}}$),

but also on ϵ_0 separately, as well as friction coefficient. The dimensionless functions obtained in turn depend on the ellipticity of the contact area via the coefficient α only (although this is the chosen approximation, not a result).

To have a full mapping between the α to best fit results for the contact ellipticity, Kalker (1972) used the matched asymptotic expansion method to expand the general three-dimensional deformation in powers of the small parameter de fining the ratio between the small and large dimensions of the contact region. The first term in this expansion is a two-dimensional solution, but the logarithmic term, corresponding here to the choice of d, is contained in the second term which for more general problems can be obtained as the solution of a line integral equation with a logarithmic kernel. In particular, the tangential compliance of an elliptical contact of semi-axes a and b will be equal to that of a two-dimensional contact of semi-width a with the same force per unit width if the latter is determined using the value

$$d = 2b \tag{23}$$

When using this approach, an extremely good fit of tangential load results from Gross-Thebing's thesis, par.7.1 ie, for an ellipticity $b/a_0 = 1.5$, was found, in Barber *et al.* (2008).

3 Coupling with the dynamics and limit cases

The dynamic equilibrium of the wheelset, which we simplify now with no stiffness or damping, gives

$$I_w \frac{d\Omega}{dt} = (Q - Q_0)\, R \tag{24}$$

where I_w is the inertia of the wheel. Moving to the oscillatory parts therefore, (24) reduces to

$$\iota\omega I_w \Omega_1 = Q_1 R \tag{25}$$

Substituting Ω_1 from (25) into (6i), and collecting Q_1, and using $\zeta = \frac{2\omega a_0}{V}$, we can write the tangential load oscillatory term in the perturbation as a function of the oscillatory term in normal load only

$$Q_1 = \frac{Q_P(\zeta)}{1 - Q_\Omega(\zeta)\frac{R}{\iota\omega I_w}} P_1 \,, \tag{26}$$

For dissipation, substituting Ω_1 from (25) into (6ii), we have

$$W_1 = W_P(\zeta) P_1 + W_\Omega(\zeta) \frac{R}{\iota\omega I_w} Q_1 \tag{27}$$

and using (26, 21, 22), we can write it in terms of normal load only

$$W_1 = \left\{ W_P(\zeta, \alpha) + W_\Omega(\zeta, \alpha) \frac{Q_P(\zeta, \alpha)}{\frac{\iota\omega I_w}{R} - Q_\Omega(\zeta, \alpha)} \right\} P_1 \tag{28}$$

The present calculation associates dissipation with the position of the wheel, whereas dissipation occur towards the rear of the contact. For this reason the lag of dissipation at a point on the rail is overstimated by about $2\pi a_0/\lambda = \zeta/2$. However, when the tractive ratio is large, dissipation occur nearer the centre of the contact area. For full sliding condition the lag of dissipation at a point on the rail is overestimated by about $\pi a_0/\lambda = \zeta/4$. In between full stick and full sliding we will assume a linear variation with the tractive ratio τ of this correction.

The limit of constant creepage assumed by Grassie and Johnson (1985) corresponds to the case where the wheel inertia is very large ($I_w \to \infty$). At the other extreme, the assumption of constant tangential load, as in Grassie and Edwards (2006) and Meehan *et al.* (2005), corresponds to the case $I_w \to 0$, where we can notice that assuming additionally $\zeta = 0$, the dissipation function is simplified considerably to nearly the negative of the normal load fluctuation

$$W_1 = -2\mu \frac{\epsilon_0^2}{\epsilon_{\max}} \left(1 - \frac{\epsilon_0}{2\epsilon_{\max}}\right) \left(1 + 2\beta \left(\frac{\epsilon_0}{\epsilon_{\max}}\right)\right) V P_1 \tag{29}$$

This is a remarkable result, since now all the locations where the normal load is highest, are automatically the locations of the highest minimum real part of dissipation.

4 Example results

Here, we use the rail vertical receptance described with a simple Euler beam model as in Afferrante and Ciavarella (2008). This simple model show a good agreement with the rail vertical receptance from Bhaskar *et al.* (1997), i.e. a continuous support typical rail for Intercity Track (the paper refers to the Vancouver SkyTrain, but in part II seems to deal with BR track constants), for the frequency of interest for corrugation (greater than about 450 Hz). We neglect effect of the pinned-pinned resonance at about 1 kHz, and also the difference between receptance mid-way between sleepers with that at a sleeper. In reality, it would be extremely easy for us to add the lower frequency range, as we have in our database quite a few vertical receptance models. However, choosing the frequency range $f > 450Hz$ permits to have a clean model, which depends only on the asymptotic value of vertical receptance obtained for a simple Euler beam model H_{rail} together with H_w, $1/k_H$ the concentrated mass receptance of the wheel, and the Hertz linearized contact stiffness, respectively

$$H_{rail} = \frac{\exp\left(-\iota 3\pi/4\right)}{2\sqrt{2}\left(m_{rail}^3 E J_{rail}\right)^{1/4} \omega^{3/2}}; \qquad H_w = -\frac{1}{M_w \omega^2}; \qquad k_H = \left[\frac{6G^2 P_0 R_e}{(1-\nu^2)}\right]^{1/3} \tag{30}$$

where m_{rail} and J_{rail} are the mass and the inertia of the section area of the rail and ω is the circular frequency.

From this, the normal load P_1 is evaluated as

$$P_1 = \frac{\Delta}{H_{rail} + H_w + 1/k_H} \tag{31}$$

where Δ is the amplitude of the corrugated profile of the rail.

Hence, it is clear that the only parameter in the model here of the rail is $m_{rail}^3 E J_{rail}$ and the supporting pad or ballast has no role at this frequency range.

The dissipation function depends on the following parameters:

- inertia of the wheel, I_w;
- steady normal load P_0;
- the tractive ratio $\tau = Q_0/\mu P_0$;
- the shape of contact area, i.e. the ratio of semi-axes b/a_0. This is taken into account in both the zero-th order coefficients via the term $\epsilon_{\max}$ which depends on Kalker's coefficient C_{00}, and in fixing the value of $d = 2b$.

For the inertia, we shall compute

$$I_w = \frac{\psi}{2} M_w R^2$$

where ψ is a factor ranging in general from 0.5 to 0.8, since the mass of the wheel M_w is concentrated near the centre because of the axle. Nielsen *et al.* (2005) for example report data range from 35 to 125 $kg\ m^2$, whereas previous traditional system may have somewhat lower values with mass of the wheel around 350 kg and hence inertia in the range $18 \div 30\ kg\ m^2$. For simplicity, we shall consider as a reference case $\psi = 0.75$ and the mass of the wheel 350 kg, with a normal load of 50 kN, as a realistic value for most systems. Reference values are summarized in table 1.

Figure 3 shows 10 equally spaced contour levels from zero to the max negative real part of dissipation function (**??**), as a function of speed and wavelength of corrugation. Regular big dots indicate the highest predicted growth for a given speed. Color lines show constant frequency 300, 1100 Hz for reference, also equal to the lines in figure 1, and its experimental data points are also included. Since the model for the rail is valid for $f > 450Hz$, the data should be taken accordingly. The shaded region denotes the zones at frequency $f < 450\ Hz$. The four plots of figure 3 are obtained for different values of d, and respectively for $d = 2b = 3a_0, 6a_0, 9a_0, 12a_0$. These limits reasonably bracket the range covered by practical variation of d, i.e. of ellipticity of the contact. The contours can be followed by looking at the points of local maxima for any given velocity, in the range of wavelengths in the figure. Notice two possible regimes of corrugation:

- *at low frequencies (around* $500 \div 600\ Hz$*)* where the wavelength of corrugation is linear with the speed V;
- *at high frequencies (*$> 1500\ Hz$*)* which compares only for elongated contact where the wavelength of corrugation is almost constant with the speed.

The results of this model in the "nearly circular case" seems surprisingly in close agreement with the experimental findings collected in figure 1 of Bhaskar *et al.* (1997), despite that considers many different systems and clearly different operating conditions spanning more than a century (old BR data and Harrison's data for British railways, Vancouver SkyTrain).

Figures 4a and 4b show the same results in a different manner, showing the effect of d i.e. of contact ellipticity is relatively mild, at least with these parameters. In particular, for the same values of the parameter d, we show the variation with the speed V of the minimum of the real part of W_1 and the frequency of corrugation, respectively. Notice the frequency of corrugation is almost constant, not too far from the Winkler results of Ciavarella and Barber (2008), and close anyway to $500 \div 600\ Hz$.

Figure 5a shows the effect of the tractive ratio $\tau = Q_0/\mu P_0$ on the expected corrugation wavelength for $d = 2b = 3a_0$. Figure 5b shows the variation of the corresponding minimum of the real part of W_1 with the speed V. The frequency of corrugation significantly reduces with the tractive ratio passing from about 500 Hz for $\tau = 0.1$ to 270 Hz for $\tau = 0.9$. Correspondingly the minimum of the real part of W_1 increases, and a new regime also appears at high frequencies.

A comparison between constant creepage (large inertia) and constant tangential force (low inertia) is proposed in figure 6, to show that the effect of assuming constant creepage, or constant tangential load, is dramatic, and explains why the Grassie-Johnson (1985) simplified model could not justify the observed corrugation. In particular, the results seem to suggest that the constant creepage predicts corrugation for very high frequency regimes. Notice however that in terms of growth rate, the constant creepage is about correct, whereas it is constant tangential load to be largely in error.

Finally, figure 7 shows the effect of the steady normal load P_0 on the expected wavelength of corrugation and on the minimum of real part of W_1. Notice the frequency of corrugation increases with the normal load P_0. Also a new regime of corrugation with almost constant wavelength at low speeds appears at high normal loads.

5 Discussion

The present model is limited in many respects:

1. it considers only longitudinal mechanisms. However, our own estimates over the difference between longitudinal and lateral creepage mechanisms (which are the subject of an ongoing investigation) do not suggest the same conclusion of Frederick (1986), who found a factor 20 more likely corrugation in lateral direction for the same creepage ratio, which probably motivated the Berlin group to look only at lateral creepage (despite the same Frederick, in the discussion of the Hempelmann and Knothe (1996) paper, suggests to include longitudinal creepage, as more likely to be much higher). Moreover, we know that longitudinal creepage can be up to 10 times higher than lateral one. Hence, since corrugation grows with the square of creepage, here we have a factor 100 in favour of the longitudinal mechanisms.

2. it neglects possible coupling between low-frequency and high-frequency, which however has often been found to be indeed negligible (Bhaskar *et al.*, 1997). In general, the corrugation phenomena can be justified if one takes an initial spectrum of roughness, and looks at the transient amplification. Since the initial spectrum contains various frequencies and in general more frequency content in the longer wavelengths, the appearance of corrugation in the short term may be different from the long term one, where one expects that nonlinearity would lead to a limit cycle. Normally, it is considered that for example, when amplitude of corrugation in the short-pitch range reaches about 80 μm there is loss of contact, but by then the noise is so large that most system maintenance strategies would have had to recur to grinding – indeed most railways grind at amplitudes of about 50 μm.

3. it does not consider discrete supports, as we have mentioned already few times. For an approximate treatment, people usually have considered local values of stiffness. This clearly is one possible approximation, and the risk is to overestimate the role of discrete supports. Considering a smoothed out continuous support model is another approximation, despite in this sense this has escaped surprisingly the attention of engineers, surprisingly since many other resonances are often neglected suggesting they are too narrow to have a role (particularly, the wheelset ones). This may be due partly to instinctive and emotional arguments, perhaps based on the fact that vertical dynamics of the vehicle has a much longer history, starting from Timoshenko already in the early years of 1900, so that people have had more time to "generalize" the Timoshenko ideas. But a careful comparison on how "narrow" are the various resonances has not been done. Indeed, when Bhaskar *et al.* (1997) looked at the continuous vs discrete model for their receptance, they noticed that the peak of discrete support pinned-pinned resonance was very narrow and decided it was not worth including this effect, and also as supported by experimental evidence. We are not saying that in other cases the effect is more marked. Still, our continuous model, with its simplicity, would be a useful term of comparison. At the very least, we can expect that, not too close to the frequency of pinned-pinned resonance, our prediction should not be completely invalid, although it is well known that parametric resonance, particularly in multi-DOF systems, has effects also remote from the

primary resonance of the system, as there are sub and super-harmonics. We have conducted some work in this area, with a simplified model (Hoffmann *et al.* 2008), but their relevance is not immediate for the practical systems under consideration.

4. it does not consider appropriate transient effects in partial slip, since we use receptance functions developed under full stick, despite the zero-th order terms are obtained from a partial slip solution.

5. it does not consider interaction between wheels in waves reflecting from one end to the other, and the many other possible mechanisms for corrugation or interactions.

6 Conclusions

Why our title "One Hundred Years of Solitude"? We have used the Gabriel Garcia Marquez expression to indicate our impression from the large (but neverthless very limited) literature review on the problem. Indeed, the different models hardly make correct estimates over the entire frequency range, so that the comparison over the "dominant" mechanism should be taken with extreme care. A lot of the conclusions were obtained in models where the assumptions were stronger than it would be needed to extrapolate the conclusions. In our modelling of the problem, perhaps because we refused almost every typical conclusion in the literature, we never had any problem to explain short-pitch corrugation. The very first model we devised (Ciavarella and Barber, 2008), already gave reasonable results, despite neglecting discrete supports, and the pinned-pinned resonance, and otherwise making only a perturbative approach to the harmonic transient rolling of a cylinder over a corrugated rail, in the simplest Winkler model approximation.

Later, we have found the closed form solution in the continuum case by means of a ad-hoc transform solution for line contact (Barber *et al.*, 2008) in full stick. Here, with an approximate "educated guess" approach, we further generalized this case for elliptical contact, and partial slip. The results show an even better correlation with experimental data on railway corrugation than the previous Winkler model, as they suggest possible growth of corrugation (for frequencies higher than 450 Hz for the simplified receptance we have used) in the range $500 \div 600$ Hz. Therefore, there is a possible explanation for the corrugation "enigma" even without to recur to the pinned-pinned resonance due to discrete supports, which is not included in the model. *The reason why Frederick (1986), and lately many other authors, seemed to have indication of this regime in their models (despite the contrary experimental evidence), was possibly partly due to the errors associated to their simplified treatment of this extremely difficult effect. The contemporary lack of a convincing alternative model to explain short pitch corrugation may have induced some authors to come to this conclusion, but we prefer to maintain a prudent agnostic view over which mechanism is dominant, as this is likely to depend on many factors, and a detailed comparison is not addressed in this paper.*

7 References

L. Afferrante Winkler partial slip solution for harmonic oscillations in steady rolling contact problems, submitted, (2008).

L. Afferrante and M. Ciavarella, On corrugation models and the "roaring rails" enigma: a simple analytical contact mechanics model based on aperturbation of Carter's solution, submitted, (2008).

A. Alonso and J.G. Giménez, Non-steady state modelling of wheel-rail contact problem for the dynamic simulation of railway wheels, Vehicle System Dynamics, Vol.45 (2007), pp. 1-18.

J.R. Barber, M. Ciavarella, L. Afferrante and A. Sackfield, Effect of small harmonic oscillations during the steady rolling of a cylinder on a plane, submitted to Journal of Sound and Vibration (2008).

A. Bhaskar, K. L. Johnson, G. D. Wood and J. Woodhouse, Wheel-rail dynamics with closely conformal contact Part 1: dynamic modelling and stability analysis IMechE Proc Instn Mech Engrs Vol. 211 Part F (1997), pp. 11-26.

R.M. Carson and K.L.Johnson, Surface corrugations spontaneously generated in a rolling contact disc machine, Wear Vol. 17 (1971), pp. 59.

F. W. Carter, On the Action of a Locomotive Driving Wheel. Proc. Roy. Soc., London, 1926, Ser.A:151-157.

M. Ciavarella and J.R.Barber, Influence of longitudinal creepage and wheel inertia onshort-pitch corrugation: a resonance-free mechanism to explain the roaring rail phenomenon Proc. IMechE, Part J: J. Engineering Tribology Vol. 222 (2008), pp. 1-11.

C. O. Frederick, A rail corrugation theory. Proceedings of the 2nd International Conference on Contact Mechanics of Rail-Wheel Systems, University of Rhode Island, (1986), pp. 181-211 (University of Waterloo Press).

S.L. Grassie and K.L. Johnson, Periodic microslip between a rolling wheel and a corrugated rail, Wear, Vol. 101 (1985), pp. 291-305.

S.L. Grassie and J. Kalousek, Rail corrugation: characteristics, causes and treatments, J Rail Rapid Transit, Proc. Inst. Mech. Eng., Vol. 207F (1993), pp. 57-68.

S.L. Grassie R.W. Gregory D. Harrison and K.L. Johnson, The dynamic response of railways track to high frequency vertical excitation, Int J Mech Sci, Vol. 24 (1982), pp. 77-90.

S.L. Grassie, Rail corrugation: advances in measurement, understanding and treatment, Wear, Vol. 258 (7-8) (2005), pp. 1224-1234

S.L. Grassie and J.W. Edwards, Development of corrugation as a result of varying normal load, 7th Int Conf on Contact Mechanics and Wear of Rail/Wheel Systems (CM2006), Brisbane, Australia, September 24-26, 2006.

A. Gross-Thebing, A lineare Modellierung des instationaren Rollkontaktes von Rad und Schiene. VDI Fortschritt-Berichte, Reihe 12, No. 199, Dusseldort, 1993.

D. Harrison Corrugation of railways. PhD Thesis, Cambridge University, UK, 1979.

N. P. Hoffmann, M. Ciavarella, C.Weiß, The effect of long-wavelength stiffness variation on wear pattern generation, submitted, (2008).

K. Hempelmann and K. Knothe, An Extended Linear Model for the Prediction of Short Pitch Corrugation. Wear, Vol. 191 (1996), pp. 161-169.

K. Hempelmann, Short Pitch Corrugation on Railway Rails – A Linear Model for Prediction. VDI Fortschritt-Berichte, Reihe 12, No. 231, Dusseldort, 1994.

J.J. Kalker, On elastic line contact, ASME Journal of Applied Mechanics, Vol. 39 (1972), pp. 1125-1132.

K.L. Johnson and G.G. Gray, Development of corrugations on surfaces in rolling contact, Proc Inst Mech Eng London, Vol. 189 (1975), pp. 45-58.

P.A. Meehan, W.J.T. Daniel and T. Campey,. Prediction of the growth of wear-type rail corrugation, Wear, Vol. 258 (7-8) (2005), pp. 1001-1013.

X. Sheng, D.J. Thompson, C.J.C. Jones, G. Xie, S.D. Iwnicki, P. Allen and S.S. Hsu , Simulations of roughness initiation and growth on railway rails Journal of Sound and Vibration Vol. 293 (3-5) (2006), pp. 819-829

T.X Wu. and D.J. Thompson, On the parametric excitation of the wheel/track system. Journal of Sound and Vibration, Vol. 278 (4-5) (2004), pp. 725-747.

T.X Wu. and D.J. Thompson, An investigation into rail corrugation due to micro-slip under multiple wheel/rail interactions. Wear, Vol. 258 (2005), pp. 1115-1125.

T.X Wu. and D.J. Thompson, On the rolling noise generation due to wheel/track parametric excitation. Journal of Sound and Vibration, Vol. 293 (3-5) (2006), pp. 566-574.

Captions for figures

Figure 1. Variation of corrugation wavelength with speed (data from Bhaskar *et al.*, 1997 fig.1). Superposed are 3 lines which refer to the most commonly frequencies associated to models of short pitch corrugation, clearly remote from most data points.

Figure 2. Coordinate system for the rotating wheel.

Figure 3. The expected corrugation wavelength for: (a) $d = 2b = 3a_0$; (b) $d = 2b = 6a_0$; (c) $d = 2b = 9a_0$; (d) $d = 2b = 12a_0$ ($P_0 = 50\ kN$; $\tau = 0.1$) (circles BR survey, 1991; triangles Harrison, 1979; crosses Vancouver 'Skytrain', 1992).

Figure 4. (a) Variation of the minimum of the real part of W_1 with the speed V for different values of the parameter d ($P_0 = 50\ kN$; $\tau = 0.1$); (b) Variation of the frequency of corrugation with the speed V for different values of the parameter d ($P_0 = 50\ kN$; $\tau = 0.1$).

Figure 5. (a) The expected corrugation wavelength for different tractive ratio τ ($P_0 = 50\ kN$; $d = 2b = 3a_0$); (b) Variation of the minimum of the real part of W_1 with the speed V for different values of the tractive ratio τ ($P_0 = 50\ kN$; $d = 2b = 3a_0$).

Figure 6. (a) The expected corrugation wavelength for different inertia: $I_w \to \infty$ (constant creepage), $I_w \to 0$ (constant tangential force), $I_w = 27.77\ kg\ m^2$ ($P_0 = 50\ kN$; $d = 2b = 3a_0$; $\tau = 0.5$); (b) Variation of the minimum of the real part of W_1 with the speed V for different inertia ($P_0 = 50\ kN$; $d = 2b = 3a_0$; $\tau = 0.5$).

Figure 7. (a) The expected corrugation wavelength for different steady normal load P_0 ($d = 2b = 3a_0$; $\tau = 0.5$); (b) Variation of the minimum of the real part of W_1 with the speed V for different P_0 ($d = 2b = 3a_0$; $\tau = 0.5$).

Young's modulus	$E = 207\ GPa$
Poisson's ratio	$\nu = 0.3$
friction coefficient	$\mu = 0.4$
wheel radius	$R = 0.46\ m$
mass of the wheel	$M_w = 350\ kg$
inertia of the wheel	$I_w = 27.77\ kg\ m^2$
mass of the rail	$m_{rail} = 56\ kg/m$
inertia of the section area of the rail	$J_{rail} = 2.35 \times 10^{-5}\ m^4$
input ripple, dispacement	$\Delta = 5\ \mu m$

Table 1. Operating parameters.

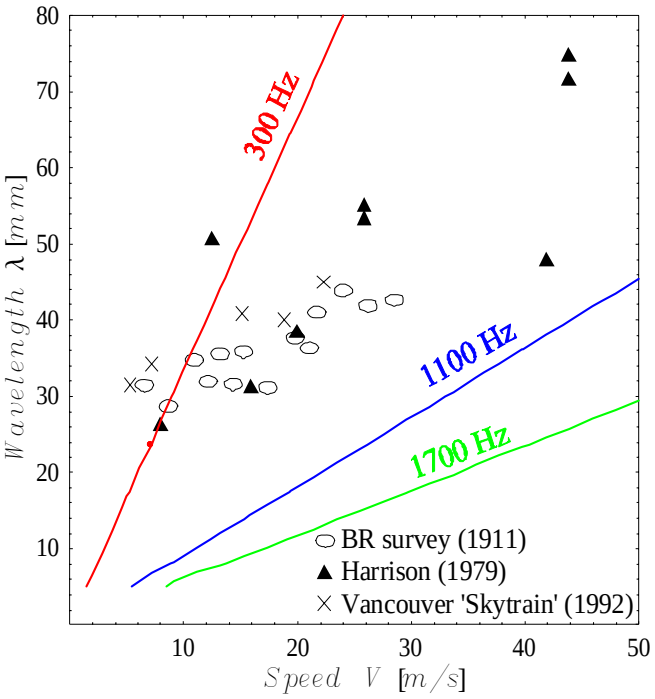

Figure 1. Variation of corrugation wavelength with speed (adapted from Bhaskar *et al.*, 1997).

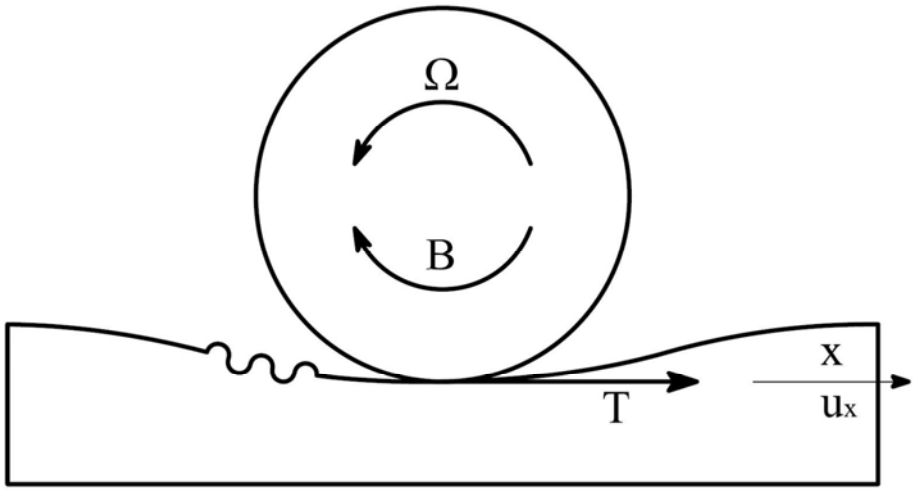

Figure 2. Coordinate system for the rotating wheel.

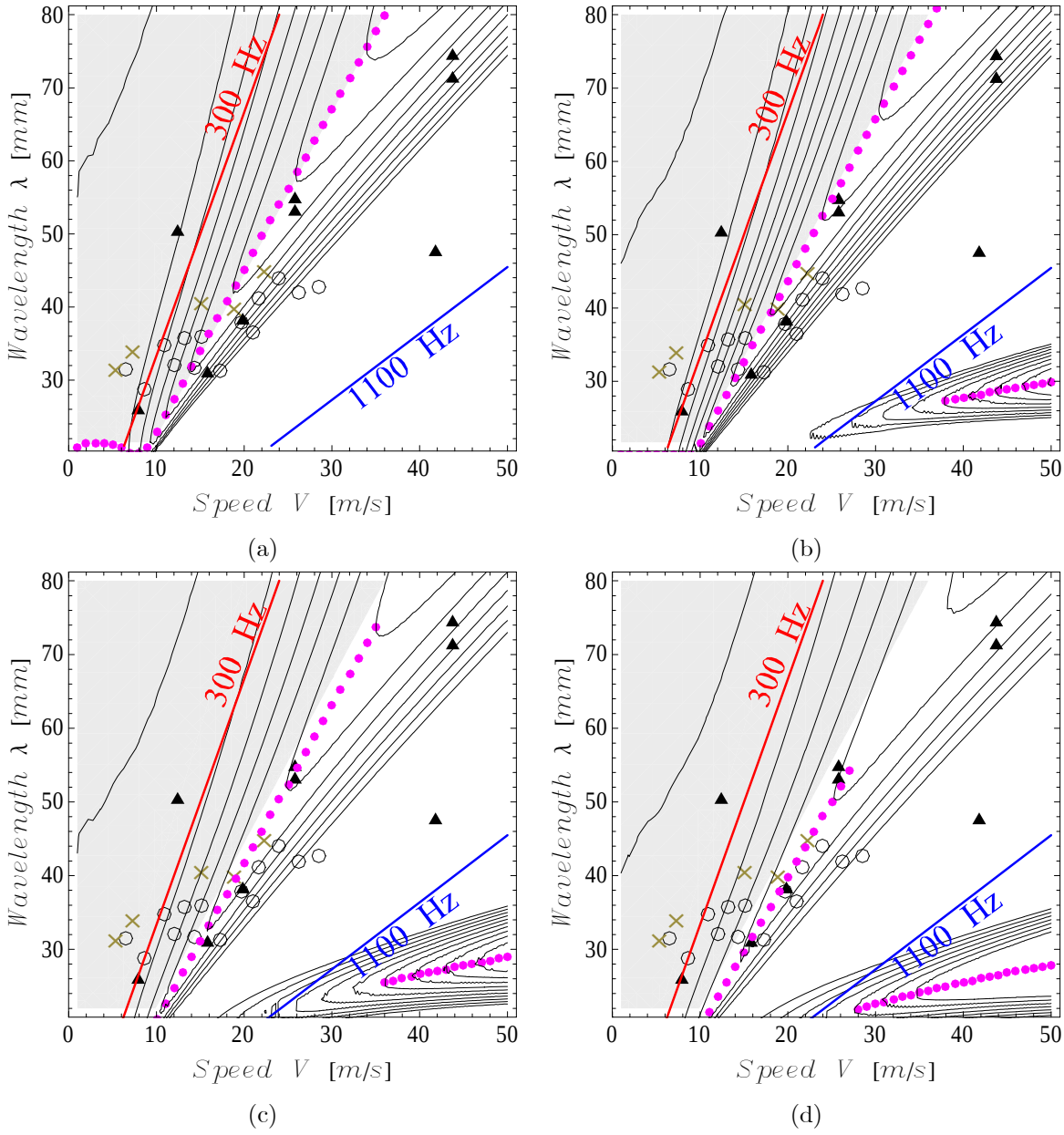

Figure 3. The expected corrugation wavelength for: (a) $d = 2b = 3a_0$; (b) $d = 2b = 6a_0$; (c) $d = 2b = 9a_0$; (d) $d = 2b = 12a_0$ ($P_0 = 50\ kN$; $\tau = 0.1$) (circles BR survey, 1991; triangles Harrison, 1979; crosses Vancouver 'Skytrain', 1992).

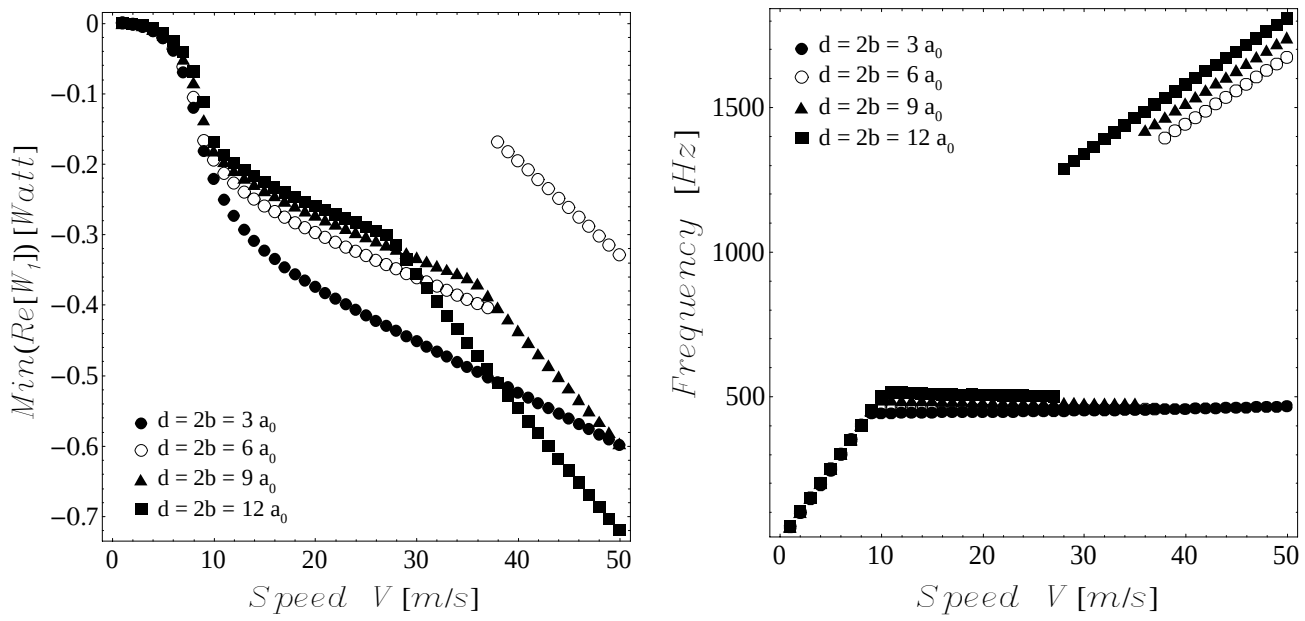

(a) (b)

Figure 4. (a) Variation of the minimum of the real part of W_1 with the speed V for different values of the parameter d ($P_0 = 50\ kN$; $\tau = 0.1$); (b) Variation of the frequency of corrugation with the speed V for different values of the parameter d ($P_0 = 50\ kN$; $\tau = 0.1$).

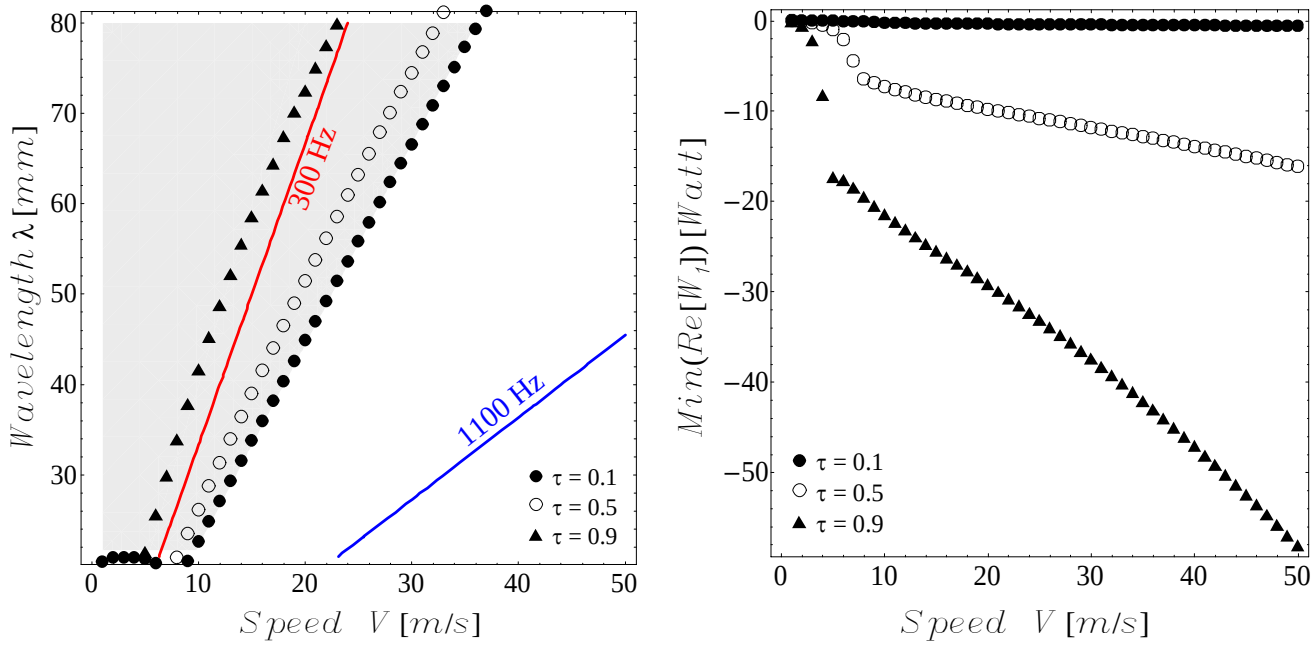

(a) (b)

Figure 5. (a) The expected corrugation wavelength for different tractive ratio τ ($P_0 = 50\ kN$; $d = 2b = 3a_0$); (b) Variation of the minimum of the real part of W_1 with the speed V for different values of the tractive ratio τ ($P_0 = 50\ kN$; $d = 2b = 3a_0$).

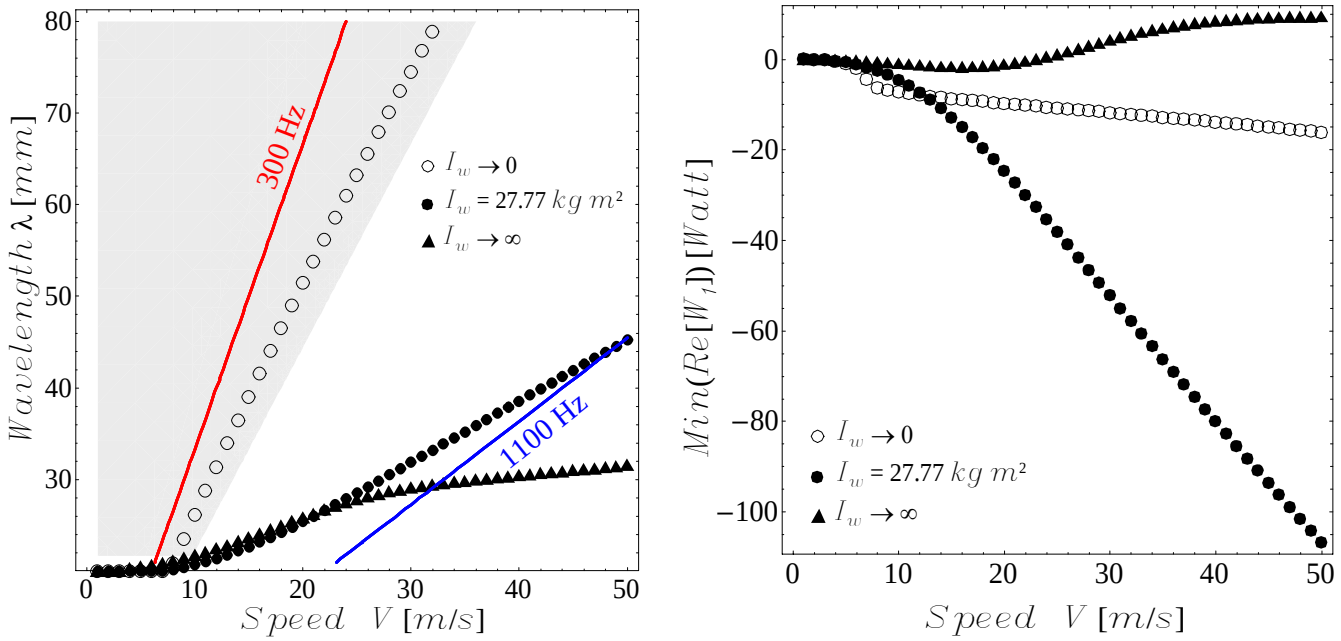

(a) (b)

Figure 6. (a) The expected corrugation wavelength for different inertia: $I_w \to \infty$ (constant creepage), $I_w \to 0$ (constant tangential force), $I_w = 27.77\ kg\ m^2$ ($P_0 = 50\ kN$; $d = 2b = 3a_0$; $\tau = 0.5$); (b) Variation of the minimum of the real part of W_1 with the speed V for different inertia ($P_0 = 50\ kN$; $d = 2b = 3a_0$; $\tau = 0.5$).

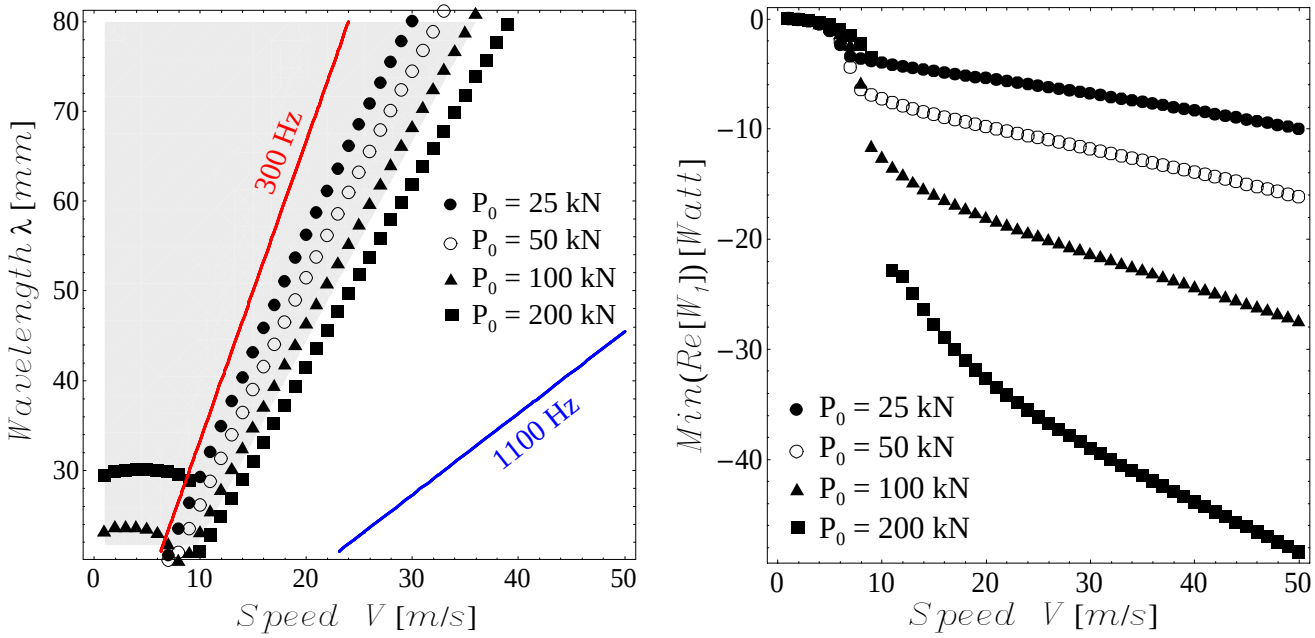

(a) (b)

Figure 7. (a) The expected corrugation wavelength for different steady normal load P_0 ($d = 2b = 3a_0$; $\tau = 0.5$); (b) Variation of the minimum of the real part of W_1 with the speed V for different P_0 ($d = 2b = 3a_0$; $\tau = 0.5$).